Journal of Ceramic Processing Research. Vol. 8, No. 5, pp. 369~375 (2007)

J O U R N A L O F
Ceramic Processing Research

Numerical investigation of the permeability level of ceramic bipolar plates for polymer electrolyte fuel cells

Chi Young Jung[b], Jay Jung Kim[a], Soo Youn Lim[b] and Sung Chul Yi[b,*]
[a]*Department of Mechanical Engineering, Hanyang University, Seoul 133-791, Korea*
[b]*Department of Chemical Engineering, Hanyang University, Seoul 133-791, Korea*

In this paper, a three dimensional, mathematical model for the analysis of the mass transfer of fuel (H_2) and oxidizer (O_2) in a polymer electrolyte fuel cell (PEFC) with solid, porous bipolar plates was developed using a commercial computational fluid dynamics code, Fluent® 6.3.26 and a CAD system CATIA®. Simulations were carried out for various permeabilities from 10^{-6} m^2 to 10^{-12} m^2 in the porous ceramic materials of the bipolar plates. By using a porous medium with a low permeability in the bipolar plates, it was possible to attain a higher and well-distributed current density compared to cases with a permeability of zero due to enhancement of the reaction area accessible by gas reactants. However, with an increase of permeability in bipolar plates from 10^{-13} m^2 to 10^{-9} m^2, the average current density decreased from 0.8497 A/cm^2 to 0.8073 A/cm^2 due to leakage of gas reactants. Consequently, an optimal permeability of bipolar plates was obtained as 4.51×10^{-9} m^2 from the standpoints of leakage and distribution of gas reactants.

Key words: PEFC, Model, CFD, Bipolar Plate, Permeability.

Introduction

A single cell of a polymer electrolyte fuel cell system consists of nine layers: anode bipolar plate, anode flow channel, anode gas diffusion layer, anode catalyst layer, proton exchange membrane, cathode catalyst layer, cathode gas diffusion layer, cathode flow channel and cathode bipolar plate [1]. PEFCs use bipolar plates to conduct electrons generated by an electrochemical reaction. As there are no materials that have zero-permeability, some investigations have been accomplished by mathematical modeling of a PEFC which regard bipolar plates as another flow path as gas diffusion layers [2, 3].

In terms of a flow-field design, it is very difficult to optimize the shape and size of a flow channel and bipolar plates since there are many factors which affect the cell performance such as the different materials used in bipolar plates [3], channel/rib ratio [4], and channel path length [5]. For this reason, it is a decisive point to set up these design parameters at optimum values in order to enhance the cell performance at fixed operating conditions.

In this paper, a model development of a steady-state, three-dimensional mathematical model for PEFCs was performed. Pointing at terms of flow-field design, such as the gas permeability effect in the anode bipolar plate and the cathode bipolar plate on the cell performance was studied with the model developed. Through this study, our main goal was to obtain an optimum value of the permeability level in bipolar plates in order to increase the uniformity in distribution of reactant species and current density over the active area.

*Corresponding author:
Tel : +82-2-2220-0481
Fax: +82-2-2298-5147
E-mail: scyi@hanyang.ac.kr

Mathemtical Model

In our present research, as illustrated in Fig. 1, a single straight-channel, three dimensional polymer electrolyte fuel cell system was considered as the computational domain. For numerical convenience, mathematical modeling was performed with a single straight-channel polymer electrolyte fuel cell. The modeled region consists of two bipolar plates, two flow channels, two gas

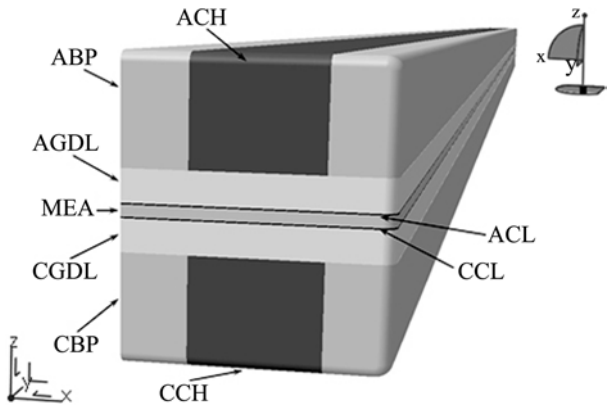

Fig. 1. Schematic of a single straight-channel polymer electrolyte fuel cell.

diffusion layers, two catalyst layers, and an electrolyte membrane. We adopted a single-domain approach, which take governing equations (1) to (4) into account through all nine regions.

Model Assumptions

The proposed model includes the following assumptions: (i) ideal gas mixtures, (ii) incompressible and laminar flow due to small pressure gradients and flow velocities, (iii) homogeneous porous gas diffusion layers and catalyst layers, (iv) a constant cell temperature condition, (v) a highly electron-conductive solid matrix, and (vi) a negligible volume of liquid-phase water in the domain.

Governing Equations

In the present paper, a single-domain model formation was used for the governing equations, which are valid for all the sub-regions used. Therefore, no interfacial conditions are used at interfaces between the components of the cell. Under the foregoing model assumptions, the governing equations can be written as below:

$$(\nabla\cdot\rho\mathbf{u})=0 \tag{1}$$

$$\frac{1}{(\varepsilon^{eff})^2}\nabla\cdot(\rho\mathbf{u}\mathbf{u})=-\nabla P+\nabla\cdot(\mu\nabla\mathbf{u})+S_u \tag{2}$$

$$\nabla\cdot(\mathbf{u}C_k)=\nabla\cdot(D_k^{eff}\nabla C_k)+S_k \tag{3}$$

$$\nabla\cdot(\kappa_e^{eff}\nabla\Phi_e)+S_\Phi=0 \tag{4}$$

The mass conservation equation is shown as Eq. (1), where ρ is the density of the gas mixture. According to the preceding assumption (ii), mass source/sink terms are ignored.

The momentum equation is shown as Eq. (2), where ε is the effective porosity inside porous mediums, and μ is the viscosity of the gas mixture. The momentum source term, S_u, is used to describe Darcy's drag for flow through porous gas diffusion layers and catalyst layers [6] as:

$$S_u=-\frac{\mu}{K}\mathbf{u} \tag{5}$$

where K is the gas permeability inside porous mediums.

The species equation is shown as Eq. (3), where D_k^{eff} is the effective diffusion coefficient of species k (e.g. hydrogen, oxygen, nitrogen and water vapor) and is defined to describe the effects of porosity in the porous gas diffusion layers and catalyst layers by the Bruggeman correlation [15] as:

$$D_k^{eff}=(\varepsilon^{eff})^{1.5}D_k \tag{6}$$

In addition, the diffusion coefficient is defined as a function of temperature and pressure [11] by the following equation:

Table 1. Transport properties [11]

Property	Value
H_2 diffusivity in the gas channel, $D^0_{H_2}$	1.10×10^{-4} m^2/s
O_2 diffusivity in the gas channel, $D^0_{O_2}$	3.20×10^{-5} m^2/s
H_2O diffusivity in the gas channel, $D^0_{H_2O}$	7.35×10^{-5} m^2/s
H_2 diffusivity in the membrane, $D^{mem}_{H_2}$	2.59×10^{-10} m^2/s
O_2 diffusivity in the membrane, $D^{mem}_{O_2}$	1.22×10^{-10} m^2/s

$$D_k=D_k^0\left(\frac{T}{T_0}\right)^{3/2}\left(\frac{P_0}{P}\right) \tag{7}$$

Transport properties for species are summarized in Table 1.

The charge conservation equation is shown as Eq. (4), where κ_e is the ionic conductivity in the ionomeric phase and has been correlated by Springer et al. [13] as:

$$\kappa_e=\exp\left[1268\left(\frac{1}{303}-\frac{1}{T}\right)\right](0.005139\lambda-0.00326) \tag{8}$$

where water content in the membrane, λ, is defined as the number of water molecules per sulfonate group inside the membrane. The water content can be expressed as a function of the water activity, a, by the following fit to experimental data [14]:

$$\lambda=0.3+6a[1-\tanh(a-0.5)]+3.9\sqrt{a}\left[1+\tanh\left(\frac{a-0.89}{0.23}\right)\right] \tag{9}$$

where the activity, a, is calculated by:

$$a=\frac{C_wRT}{P_w^{sat}} \tag{10}$$

By the Bruggeman correlation [15], the proton conductivity in the catalyst layers is defined as:

$$\kappa_k^{eff}=\varepsilon_m^{1.5}\kappa_e \tag{11}$$

where ε_m is the volume fraction of the membrane-phase in the catalyst layer.

The source/sink terms, S_k, S_Φ, in Eq. (3) and (4) over nine regions of the domain are given in Table 2.

Using the electrolyte-phase potential, Φ_e, obtained

Table 2. Source/sink terms for momentum, species, and charge conservation equations for individual regions

	Momentum	Species	Charge
Bipolar plates	$S_u=-\frac{\mu}{K}\mathbf{u}$	$S_k=0$	$S_\Phi=0$
Flow channels	$S_u=0$	$S_k=0$	$S_\Phi=0$
Gas diffusion layers	$S_u=-\frac{\mu}{K}\mathbf{u}$	$S_k=0$	$S_\Phi=0$
Catalyst layers	$S_u=0$	$\mathrm{Sk}=-\nabla\cdot\left(\frac{n_d}{F}I\right)-\frac{s_k j}{nF}$	$S_\Phi=j$
Membrane	$S_u=0$	$\mathrm{Sk}=-\nabla\cdot\left(\frac{n_d}{F}I\right)$	$S_\Phi=0$

from Eq. (4), it is possible to calculate the electrolyte-phase potential gradient in the membrane. Finally, the local current density in the membrane can be obtained from:

$$I=-\kappa_e \nabla \Phi_e \tag{12}$$

Then the average current density is calculated as follows:

$$I_{avg}=\frac{1}{A}\int_{A_{mem}} I dA \tag{13}$$

where A is the active area over the MEA.

Water Transport

In polymer electrolyte fuel cells, due to the properties of polymer electrolyte membrane, the water molecules are transported via electro-osmotic drag in addition to the molecular diffusion. Water molecules are transported through the polymer electrolyte membrane by the H^+ protons, and this transport phenomenon is called electro-osmotic drag. In addition to the molecular diffusion and electro-osmotic drag, water vapor is also produced in the cathode catalyst layer due to the oxygen reduction reaction.

Water transport through the polymer electrolyte membrane is determined from the following conservation equation:

$$\nabla \cdot (D_{H_2O}^{mem} \nabla C_{H_2O}^{mem}) - \nabla \cdot \left(\frac{n_d}{F}\mathbf{i}\right)=0 \tag{14}$$

where n_d and $D_{H_2O}^{mem}$ are the water drag coefficient from anode to cathode and the diffusion coefficient of water in the membrane phase.

The water drag coefficient is defined as the number of water molecules transported by each hydrogen proton H^+. The water drag coefficient can be determined from the following equation [14]:

$$n_d=\begin{cases} 1 & \lambda<9 \\ 0.117\lambda-0.0544 & \lambda\geq 9 \end{cases} \tag{15}$$

The diffusion coefficient of water in the polymer membrane is highly dependent on the water content of the membrane and is obtained by the following fits of the experimental data [17]:

$$D_w^{mem}=\begin{cases} 3.1\times10^{-7}\lambda(e^{0.28\lambda}-1)e^{(-2346/T)} & \text{for } 0<\lambda\leq 3 \\ 4.17\times10^{-8}\lambda(1+161e^{-\lambda})e^{(-2346/T)} & \text{otherwise} \end{cases} \tag{16}$$

Boundary Conditions

Eq. (1) through (4) form the complete set of governing equations for the conventional mathematical model. Boundary conditions are only required at the external boundaries due to the single-domain model approach used in this model. The no-flux conditions are applied for mass, momentum, species and potential conservation equations at all boundaries except for inlets and outlets of the anode and cathode flow channels. At the flow channel inlets, inlet velocities and the species concentrations are specified as:

$$\mathbf{u}_{in,a}=\frac{\zeta_a I_{ref} A_{MEA}}{2C_{H_2,in}FA_{ch}}, \quad \mathbf{u}_{in,c}=\frac{\zeta_c I_{ref} A_{MEA}}{4C_{O_2,in}FA_{ch}} \tag{17}$$

where I_{ref} is the reference current density and ζ is a stoichiometric ratio, which is defined as the ratio between the amount supplied and the amount required of the fuel based on the reference current density. The species concentrations of flow inlets are determined by the humidification conditions of both the anode and cathode inlets.

Numerical Procedures

In this research, mathematical modeling and simulation of a three dimensional PEFC were performed with a commercially available CFD code, FLUENT. However, since FLUENT does not present an electrochemical modeling module, whole governing equations except the momentum conservation equation were solved using User Defined Functions (UDFs).

It should also be mentioned that although some species do not flow in certain regions of the PEFC, the species transport equations can still be applied throughout the entire computational domain using the large source term technique originally proposed by Voller [16].

Approximately 112,000 computational cells were found to be adequate and used for all simulations. Over 400 iterations, about one-hour iteration time, were taken to reduce each residual value below 10^{-8}.

Results and Discussion

Model validation

Validation of the proposed model was carried out by a comparison with the experimental data of Wang et al. [9]. As mentioned above, the system is a single straight-channel PEFC and the geometric parameters are given in Table 3. Operating conditions were specified as a cell temperature of 70°C, a pressure of 3 atm for the anode and cathode side, and fully humidified inlet

Table 3. Geometric Parameters of PEFC [9]

Dimension	Value
Gas channel length	7.0×10^{-2} m
Gas channel width and depth	1.0×10^{-3} m
Bipolar plate width	5.0×10^{-4} m
Gas diffusion layer thickness	3.0×10^{-4} m
Catalyst layer thickness	1.29×10^{-5} m
Membrane thickness	1.08×10^{-4} m

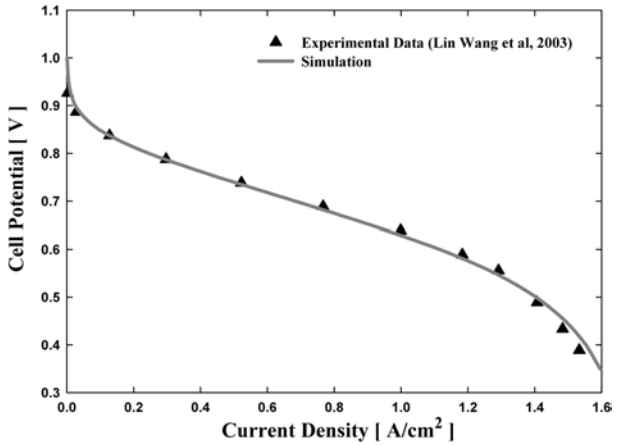

Fig. 2. Measured and predicted cell polarization curves at 70°C and 3 atm, fully humidified inlets at 70°C, and an anode/cathode stoichiometry ratio of 1.8/1.4 at 1.5 A/cm^2.

species at the given cell temperature. The multi-component mixture fluid velocities at the anode and cathode inlets have constant values corresponding to an anode/cathode stoichiometric ratio of 1.8/1.4 at the fixed reference current density of 1.5 A/cm^2.

Figure 2 shows a comparison of the calculated polarization curve and the experimental data. The predicted polarization curve shows good agreement with the experimental data.

Investigation of the bipolar plate (BP) permeability effect on cell performance was performed using the proposed model. Simulations were carried out from a BP permeability of 10^{-14} m^2 to 10^{-8} m^2 to obtain an optimal BP permeability, which enhances the cell performance by reaching a homogeneous current density distribution.

Effect of permeability levels of porous ceramic BP

Figure 3, 4, and 5 show velocity contours of the mixture fluid in the ABP and ACH when permeability values of the ABP are 10^{-12} m^2, 10^{-10} m^2, and 10^{-8} m^2 respectively. A high permeability level indicates a tendency to loose fuel from the flow channel. In the case of a highly porous ceramic bipolar plate, the gas fuel has a greater chance to leak out of the ACH, and hence promote a mass transport limit due to fuel reduction. These three figures show the gradual decrease of velocity of the mixture fluid in all of the

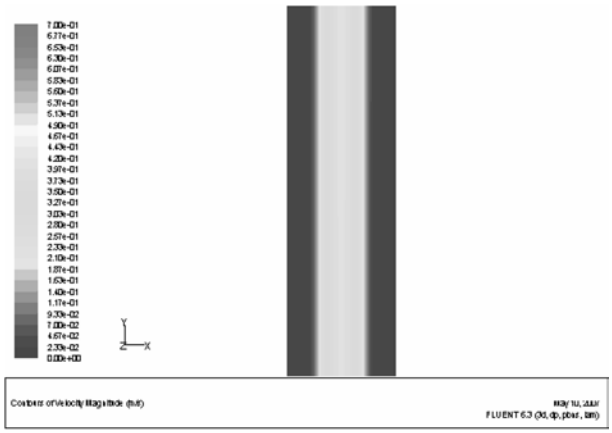

Fig. 3. Velocity contour in the anode flow channel when BP permeability is 10^{-12} m^2.

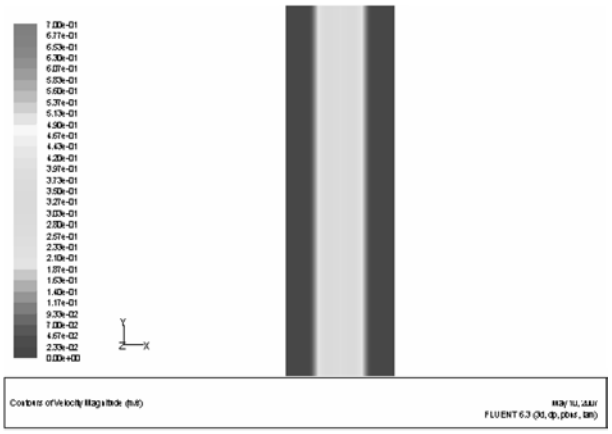

Fig. 4. Velocity contour in the anode flow channel when BP permeability is 10^{-10} m^2.

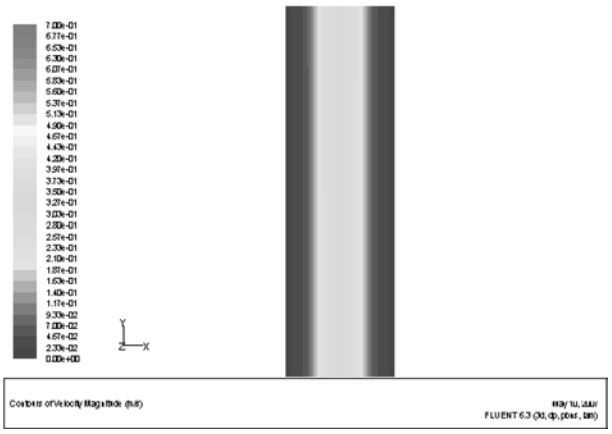

Fig. 5. Velocity contour in the anode flow channel when BP permeability is 10^{-8} m^2.

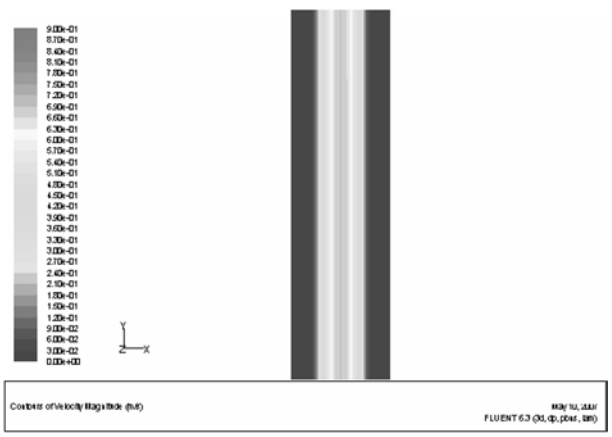

Fig. 6. Velocity contour in the cathode flow channel when BP permeability is 10^{-12} m^2.

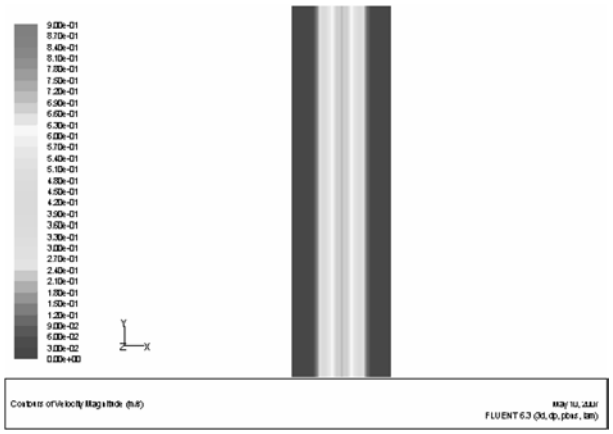

Fig. 7. Velocity contour in the cathode flow channel when BP permeability is 10^{-10} m^2.

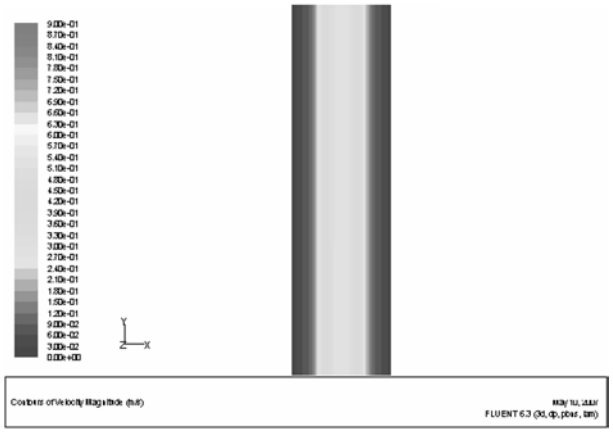

Fig. 8. Velocity contour in the cathode flow channel when BP permeability is 10^{-8} m^2.

ACH with an increase of gas permeability. Figure 6, 7, and 8 are the velocity contours of the mixture fluid in the CBP and CCH. These figures show a similar tendency to the anode flow-field. With these results, it can be concluded that a low gas permeability level is required at BP for the purpose of maximizing fuel gas usage. As a result, zero gas permeability at BP is the optimal value.

However, there is another factor to consider in optimizing channel design based on the concept of the gas permeability. This is maximizing the usage of active area, which is the effective gas/catalyst contact area out of the total electrode area. Maximizing the active area can increase unused gas/catalyst contact area. Since the shape and size of the flow channel are fixed, a valid gas permeability value can be quite an important factor in increasing the active area. Figure 9 shows four simulated results with our model. A dashed line shows the tendency for the average current density value to decrease with a decrease in gas permeability. This tendency is closely related to the reason given above. However, what should be noted is that there is a threshold point between 10^{-10} m^2 and 10^{-9} m^2. An optimal value of gas permeability is zero from the viewpoint of fuel usage but the graph shows an exceptional case. An average current density value at 10^{-12} m^2 is higher than that of a non-porous flow-field. This exceptional result is due to usage of the active area.

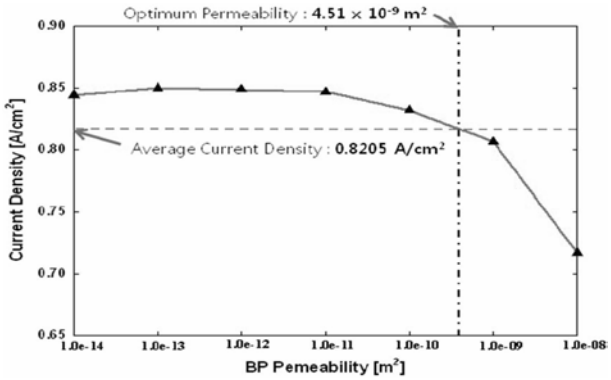

Fig. 9. Calculated current density at various permeability values of porous ceramic bipolar plates.

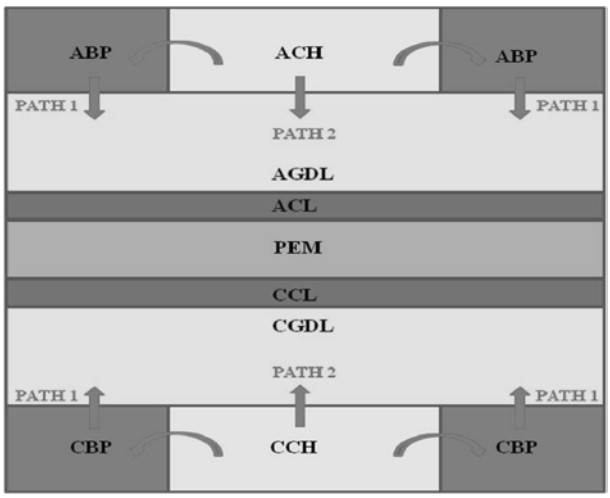

Fig. 10. Gas transport pathways in porous ceramic BP.

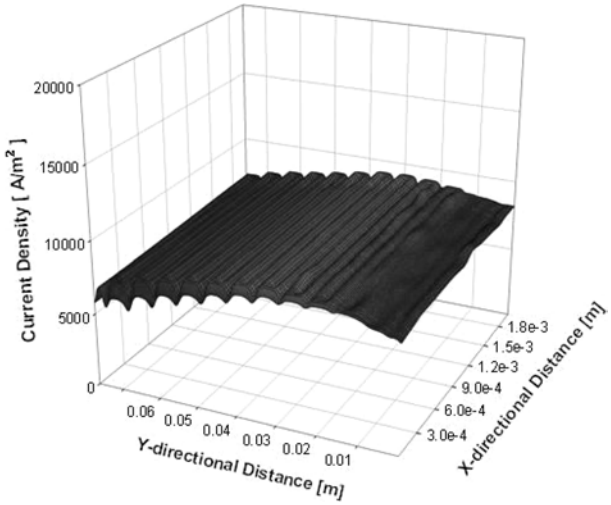

Fig. 11. Current density distribution when a non-gas-permeable BP is used.

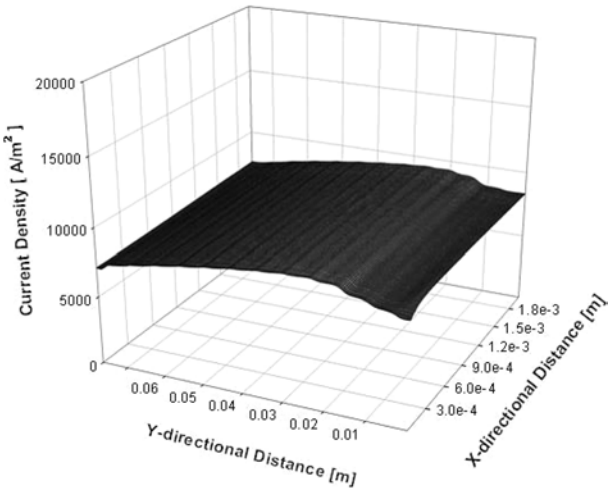

Fig. 12. Current density distribution when the BP permeability is 10^{-12} m^2.

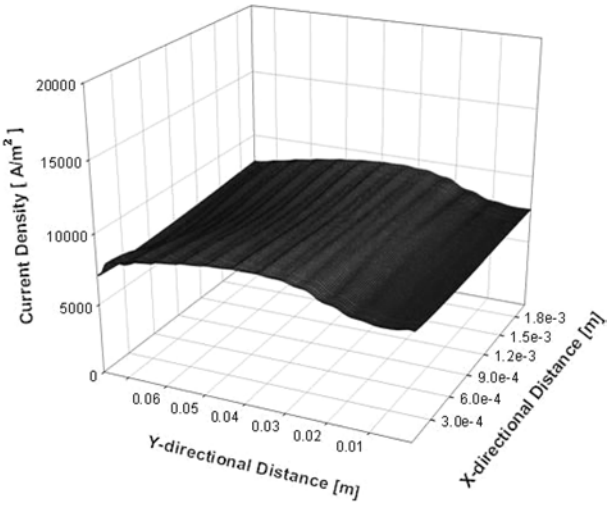

Fig. 13. Current density distribution when the BP permeability is 10^{-10} m^2.

Figure 10 shows the pathways of hydrogen and oxygen from the flow channel/bipolar plate to the gas diffusion layer. If the bipolar plate is made of non-porous material, hydrogen and oxygen diffuse only through path 1, which is the direct path from the gas flow channel to the gas diffusion layer. However, both paths 1 and 2 should be considered if a porous ceramic material is used. Path 2 stands for an additional pathway to the gas diffusion layer. If the fuel gas has a greater chance to be distributed with an increase of pathways, this means it is possible to use a larger interfacial area between the gas diffusion layer and the catalyst layer. However, more chance to diffuse through path 2 also means more chance to be well distributed. Consequently there is an optimal range in maximizing the active area with the compensating fuel leakage.

Figure 11 shows the local current density distribution on a catalyst layer when a non-porous flow channel is used. As shown here, the local current value close to the rib is lower than that of the groove. This means the electrode area close to "PATH 1" (see Fig. 10) is not used efficiently.

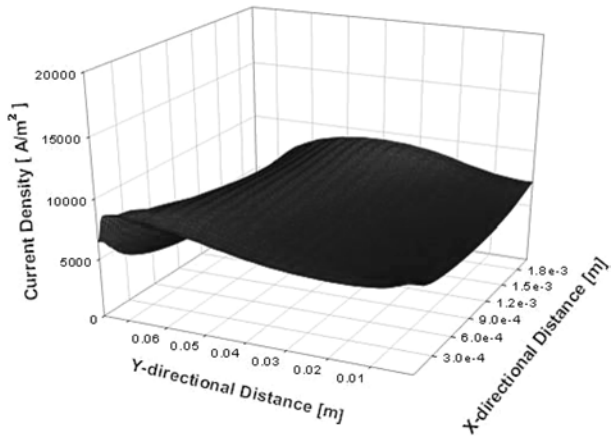

Fig. 14. Current density distribution when the BP permeability is 10^{-8} m^2.

Figure 12, 13 and 14 show the calculated current density distributions on a catalyst layer with different gas permeabilities. Among these results, Fig. 12 shows the most well-distributed current density. This means fuel leakage and flow distribution are not efficiently controlled with an increase of permeability.

Conclusions

A three dimensional, isothermal and steady-state mathematical model for a polymer electrolyte fuel cell (PEFC) was developed based on the single-domain approach. From a comparison with experimental polarization curve data [9], the developed model was validated under cell temperature and pressure conditions of 70 °C and 3 atm. Using this developed model, simulations were carried out using various permeabilities of the ceramic materials in the flow-field ranging from 10^{-6} to 10^{-12} m^2. With low gas permeability in the bipolar plates in the flow-field, it was possible to get a high and well-distributed current density compared to non-gas-permeable bipolar plates. However, the average current density value gradually decreased with an increase of gas permeability in the rib. Although zero gas permeability might be the optimal value from the viewpoint of fuel usage, we could deduce that a low gas permeability into the rib helps the cell performance and current distribution, since proper gas permeability can increase the active area. Consequently, we could deduce that there is an optimal permeability value in every design of flow-field; the value was 4.51×10^{-9} m^2 and corresponding current density of 0.8205 A/cm^2 in this study.

Acknowledgements

This research is supported by the *Undergradute*

Research Innovation Program (URIP) from Hanyang Fusion Materials and the authors gratefully appreciate it.

Nomenclature

List of symbols

a : water activity
A_{cv} : specific surface area
ABP : anode bipolar plate
ACH : anode flow channel
$AGDL$: anode gas diffusion layer
ACL : anode catalyst layer
BP : ipolar plate
C : molar concentration [mol/m^3]
CBP : cathode bipolar plate
CCH : cathode flow channel
$CGDL$: cathode gas diffusion layer
CCL : cathode catalyst layer
D : mass diffusion coefficient [m^2/s]
F : Faraday constant [C/mol]
I : local current density [A/m^2]
I_o : exchange current density [A/m^2]
β : hydraulic permeability [m^2]
M : molecular weight (or equivalent weight) [kg/mol]
n_d : electro-osmotic drag coefficient
P : pressure [Pa]
PEM : proton exchange membrane
R : universal gas constant [J/mol·K]
t : thickness [m]
T : temperature [K]
$\vec{u}$: velocity vector
V_{cell} : cell voltage
V_{oc} : open-circuit voltage
X : mole fraction

Greek Letters

α : net water transfer coefficient
η : local overpotential [V]
λ : water content
ρ : density [kg/m^3]
μ : viscosity [kg/m·s]
σ : proton conductivity [S/m]

Superscripts

op : Operating
s : Surface
sat : Saturated

Subscripts

a : Anode
c : Cathode
i : Species
k : anode or cathode
m : Membrane
ref : reference value
w : Water

References

1. Chi Seung Lee and Sung Chul Yi, Korean J. Chem. Eng. 21 (2004) 1153-1160.
2. Chi Seung Lee, Chang Hyun Yun, and Byung Moo Kim, Se Chan Jang and Sung Chul Yi, J. Ceramic Processing Research 6[2] (2005) 188-195.
3. A. Kumar and R.G. Reddy, J. Power Sources 114 (2003) 54-62.
4. S. Shimpalee and J.W. Van Zee, Int. J. Hydrog. Energy 32[7] (2007) 842-856.
5. S. Shimpalee, S. Greenway, and J.W. Van Zee, J. Power Sources 160 (2006) 398-406.
6. V. Garau, H. Liu, and S. Kakac, AIChE J. 44[11] (1998) 2410-2422.
7. Sukkee Um, C.Y. Wang, and K.S. Chen, J. Electrochem. Soc. 147 (2000) 4485-4493.
8. S. Dutta, S. Shimpalee, and J.W. Van Zee, Intl. J. Heat and Mass Trasfer 44 (2001) 2029-2042.
9. L. Wang, A. Husar, T. Zhou, and H. Liu, Int. J. Hydrog. Energy 28[11] (2003) 1263-1272.
10. T.V. Nguyen and R.E White, J. Electrochem. Soc. 140 (1993) 1218-1225.
11. R. Byron Bird, Warren E. Stewart, and Edwin N. Lightfoot, in "Transport Phenomena" (John Wiley & Sons, Inc, 1960)
12. Suhas V. Patankar, Numerical Heat Transfer and Fluid Flow, Hemisphere Publishing Corporation (1980).
13. T.E. Springer, T.A. Zawodzinski, and S. Gottesfeld, J. Electrochem. Soc. 138 (1991) 2334-2342.
14. A.A. Kuklikovsky, J. Electrochem. Soc. 150[11] (2003) A1432-A1439.
15. R.E. Meredith and C.W. Tobias, in "Advances in Electrochemistry and Electrochemical Engineering 2", (Tobias, C.W., ed., Interscience Publishers, New York, 1960).
16. V.R. Voller, Numer. Heat Transfer, Part B 17 (1990) 155.
17. S.W. Yeo and A. Eisenberg, J. Appl. Polym. Sci. 21 (1997) 875.